Computational Modeling of Dielectric Membranes for Particle Detectors

Maarten Kruis

Supervisors:
Neil Budko
Kees Hagen

October 5, 2017

Abstract

In this paper two ways of modeling the secondary electron yields of an insulator under electron irradiation, are discussed and coupled. The drift-diffusion-reaction model is used to investigate the secondary yields and charging effects.

This paper is part of the BSc Applied Physics and BSc Applied Mathematics at the Delft University of Technology.

Contents

Chapter 1

Introduction

At present, when someone wants to detect electrons (or a single electron), one needs a photomultiplier tube (PMT) to do this. A PMT is typically a vacuum glass tube with several dynodes and one anode inside. When a primary electron falls on the PMT, the electron goes via the focusing electrode to the first dynode, which works as a electron multiplier. The second dynode is held at a higher potential than the first, so the second dynode attracts the secondary electrons from the first dynode. This process continues until the secondary electrons arrive at the anode. Each dynode contributes about ~ 5 secondary electrons for each electron that falls on its surface. When the anode is for instance coupled to an oscilloscope a clear peak in current can be distinguished. This peak occurs about $\sim 50ns$ after the electron falls on the PMT.

The Imaging Physics department of the faculty of Applied Sciences at the TU Delft is attempting to create a new measuring device for electrons. This device utilizes the fact that disturbances in the charge densities in insulators do not instantaneously even out (like in a metal). This means that when an electron falls on the surface of a dielectric, a cascade of secondary electrons is created, which cannot flow away instantaneously. When a secondary electron inside the insulator comes close to the surface of the dielectric and has a kinetic energy higher than the work function, this secondary electron can leave the dielectric. When a thin membrane of a dielectric can realize a high secondary transmission yield, when an electron falls on its surface, the material can be used as a tynode (transmission dynode). This means that a setup, with several tynodes stacked on top of each other, with a vacuum and a potential difference between them, could work as an electron multiplier. A big advantage of this technique would be that a much smaller device could be used to detect electrons. This means that it would be possible to make a camera that can detect single electron impacts on a surface.

Currently there are two ways to model the physical processes inside an insulator under electron radiation The first method is tracking electron paths with Monte-Carlo simulations. The second method is a self-consistent drift-diffusion-reaction (DDR) model. This paper attempts to clarify the connection between these two models. This is done by coupling both models to the Boltzmann Transport Equation (BTE). Further, the DDR model is employed here

to simulate charging processes in continuously irradiated dielectric membranes. The original computer code was modified to include polynomial interpolation of tuned penetration depths for primary (incoming) electrons. Reflection and transmission yields are calculated for different energies of incoming electrons and different membrane thicknesses. It is shown that the charging of the membrane leads to the drop in the transmission yield over time. However, if the membrane is grounded, the yield may recover.

This paper is part of the BSc Applied Physics and BSc Applied Mathematics at the Delft University of Technology.

Chapter 2

Electron irradiation of an insulator

The information in this chapter is taken from reference [3]. This chapter attempts to describe the different stages of the processes inside an insulator, after an electron has fallen onto the surface of said insulator. Due to the primary electron a cascade of secondary excitations occur inside the insulator of which the different stages in the time interval of $10^{-18} - 10^{-7}$ are described. During the time interval the number of secondary excitations increases enormously and the average energy decreases. The stages are as follows:

$10^{-18} - 10^{-17}$s During the first attoseconds the primary impact occurs alongside Auger ionization of the insulator. Generation of secondary electrons, holes, plasmons and exitons also occur. During this stage the attosecond electron conductivity dominates.

$10^{-17} - 10^{-14}$s In this stage secondary electron-electron (e-e) and electron-hole (e-h) collisions occur and the electron energy spectrum evolves to the instantaneous distribution. When the electrons and holes lose their ability to ionize the medium, the formation of the instantaneous spectrum also stops. The electrons and holes are now ionization passive, which means that electrons can no longer impact ionize and holes are no longer able to Auger ionization. During this stage the femtosecond high-energy conductivity prevails and the charge carriers consist mainly of electrons with kinetic energy 20-10000eV.

$10^{-14} - 10^{-12}$s Due to electron phonon (e-ph) collisions the energy of the ionization passive electrons relaxes. The main charge carriers are ionization passive electrons and holes with energies between 0.1 and 20eV. The charge carriers are unable to form new electron-hole pairs. In this stage the picosecond high-energy conductivity prevails.

$10^{-12} - 10^{-11}$s During this stage the electrons and holes thermalize and the low-energy electron conductivity prevails.

$10^{-11} - 10^{-7}$s In this stage multiple trapping and detrapping of thermalized electrons and holes occur.

Chapter 3

Two models

The processes occurring in a material under electron radiation can be modeled in two ways. At the department of Imaging Physics at the TU Delft a Monte Carlo approach is used. At the department of Numerical Mathematics a Drift-Diffusion-reaction model is used. In this chapter both models are described and subsequently coupled. This is done by coupling both models to the Boltzmann transport equation (BTE).

3.1 Monte-Carlo model

With the Monte-Carlo model a realization of an electron path is calculated. From the starting point of the electron, discrete time steps are taken. At each time step one of three processes is used (The model as it is used at the time of writing this paper models 3 processes inside the material). The three precesses are:

1. Inelastic collisions
2. Phonon scattering for electrons with energy below 100 eV
3. Mott scattering for electrons with energy above 100 eV

In an inelastic collision the electron loses some energy and its direction can be changed. The angle of the new direction with respect to the old direction can be calculated with the law of conservation of momentum and energy. When an electrons scatters on a phonon only the direction of the electron changes. This is also the case for Mott scattering, except that for this process the electron bends around the electric field of an electron. Each process has a different distribution function, which only differs by one parameter. This parameter is the mean free path (λ), with for each process a different λ. Now the mean free path for the total process is:

$$\frac{1}{\lambda_{tot}} = \sum_i \frac{1}{\lambda_i} \tag{3.1}$$

The distribution function is:

$$p(L) = \frac{1}{\lambda_{tot}} e^{\frac{L}{\lambda_{tot}}} \tag{3.2}$$

With L the free path. To determine which process was used a number from a uniform distribution is pulled. The numbers that can be pulled are between 0 and $\frac{1}{\lambda_{tot}}$. This number line is divided into two parts. λ_1 is always in there, but depending on the energy of the electron λ_2 or λ_3 is used. When the process which is being used is known, it is possible to pull a number out of the angle distribution of the process. If the collision is inelastic, an energy difference has to be pulled from a distribution. The path of the electron ends, when the electron is outside of the material or when its energy has gotten too low to leave the material. An electron cannot leave the material when its kinetic energy is lower than the work function of the material.

The Monte-Carlo model described in this section is not accounting for charging phenomena due to electron/hole trapping in a material. It is possible to implement this, but the implementation would drastically slow down simulations.

3.2 Drift-Diffusion-Reaction model

The DDR model consists of a Poisson equation coupled to the carrier continuity equations and the drift-diffusion equations, along with appropriate boundary and initial conditions. The carrier continuity equations and the drift-diffusion equation can be derived from the BTE. For Poisson's equation for the potential a derivation can be found in the appendix. The Poisson equation is given by:

$$-\nabla \cdot (\epsilon \nabla V) = \frac{q}{\epsilon_0} \left(C + p - n - n_T \right) \tag{3.3}$$

where C is the density of empty traps, $n(\boldsymbol{x}, t)$ is the density of free electrons, $n_T(\boldsymbol{x}, t)$ is the density of trapped electrons and $p(\boldsymbol{x}, t)$ is the density of free holes. Poisson's equation is needed to determine the potential inside the entire domain.

3.2.1 Boltzmann transport equation

The Boltzmann transport equation (BTE) can describe the statistical behavior of a thermodynamic system, which is not in a state of equilibrium. Instead of considering the positions and momenta of individual particles in a fluid to describe the behavior of a system, the BTE uses probability distributions for position and momenta of a single particle to describe the system. For each particle species a BTE is needed. The BTE is given by:

$$\frac{\partial f}{\partial t} + \boldsymbol{F} \cdot \frac{\partial f}{\partial \boldsymbol{p}} + \frac{\boldsymbol{p}}{m} \cdot \nabla f = \left(\frac{\partial f}{\partial t} \right)_{coll} \tag{3.4}$$

where $\boldsymbol{F}$ is the force field acting on the particles, $\boldsymbol{p}$ is the momentum and and m is the mass of the particles involved. The expression $\left(\frac{\partial f}{\partial t} \right)_{coll}$ models all the collision processes in the fluid. The distribution f is a function of time, position and momentum. When the system under investigation is in the domain $\mathcal{D}$ and

$$\int_{\mathcal{D}} \int_{\mathbb{R}^3} f(\boldsymbol{r}, \boldsymbol{p}, t) \mathrm{d}^3 r \mathrm{d}^3 p = 1 \tag{3.5}$$

f is a probability distribution of a single particle in the system. In this situation $f(\boldsymbol{r}, \boldsymbol{p}, t)$ gives the probability that a particle occupies an infinitesimally small region of phase space $\mathrm{d}^3\boldsymbol{r}\mathrm{d}^3\boldsymbol{p}$ around $\boldsymbol{r}$ and $\boldsymbol{p}$ at time t. Consequently, when the distribution is normalized to the amount of particles in the system, $f(\boldsymbol{r}, \boldsymbol{p}, t)$ is the expected amount of particles in an infinitesimally small region of phase space around $\boldsymbol{r}$ and $\boldsymbol{p}$ at time t. A good example of a system that the BTE can describe is the heat flow in a system with temperature gradients. In the model that is derived below there are particle density gradients in the material, which cause a particle flow in the material. All the kinematics in the Boltzmann transport equation are classical, but the collision term can take quantum mechanics into account. This means that the BTE gives a semi-classical description of a system.

In this paper the BTE is used to describe the transport of charge carriers inside a dielectric, under electron radiation. The charge carriers in a dielectric are electrons and holes. This means that two Boltzmann transport equations are needed. One for the electrons and one for holes. This is indicated with a subscript q in the distribution function. The BTE for charge carriers with charge q is as follows:

$$\frac{\partial f_q}{\partial t} + \boldsymbol{F} \cdot \nabla_p f_q + \boldsymbol{v} \cdot \nabla f = \mathcal{Q}(f_q) - \mathcal{T}(f_q) \tag{3.6}$$

where $f_q = f_q(\boldsymbol{r}, \boldsymbol{p}, t)$ is the distribution function for a carrier with charge q. In this context q can be either e for holes and $-e$ for electrons, where e represents the elementary charge. Further more the following notation is used for the momentum-nabla operator:

$$\nabla_p = \begin{pmatrix} \dfrac{\partial}{\partial p_x} & \dfrac{\partial}{\partial p_y} & \dfrac{\partial}{\partial p_z} \end{pmatrix}^T \tag{3.7}$$

The distribution $f_q(\boldsymbol{r}, \boldsymbol{p}, t)$ is normalized, such that:

$$N = N_q = \int_{\mathcal{D}} \int_{\mathbb{R}^3} f_q(\boldsymbol{r}, \boldsymbol{p}, t) \mathrm{d}^3 r \mathrm{d}^3 p \tag{3.8}$$

Where N is the total number of carriers in the material. $N = N_q$, because the number of electrons is the same as the number of holes in a neutral material. The domain $\mathcal{D}$ is the volume of the material under observation. The expression of $\left(\frac{\partial f}{\partial t}\right)_{coll}$ is divided into two parts:

$$\left(\frac{\partial f}{\partial t}\right)_{coll} = \mathcal{Q}(f_q) - \mathcal{T}(f_q) \tag{3.9}$$

The $\mathcal{Q}$ operator takes care of the scattering processes in the material. While the $\mathcal{T}$ operator describes the generation/recombination processes in the material. $\boldsymbol{F}$ is the the force exerted on the particle by the local electric field. This means that $\boldsymbol{F} = q\boldsymbol{E}$, with q the charge of the carrier and $\boldsymbol{E}$ the electric field. $\boldsymbol{v}$ is the group velocity.

3.2.2 Method of Moments and Approximations

To derive the carrier continuity equations and the drift-diffusion equations, the method of moments is used on the BTE. For the method of moments an equation

is multiplied by a weight function, which can be raised to an integer power and is subsequently integrated over a volume. In the case of the BTE, the equation is multiplied by a weight function, which depends on the momentum of the particle and is subsequently integrated over momentum phase space. The carrier continuity equations arise when the weight function is a constant with value 1. The drift-diffusion equations arise when the weight function is the velocity $\boldsymbol{v}$. To use the method of moments on the BTE, an approximation for the collision term $\mathcal{Q}(f_q)$ is needed. The approximation that is taken in this paper is the Bhatnagar, Gross and Krook (BGK) approximation, which can be stated as follows:

$$\mathcal{Q}(f_q) \approx \frac{f_{q,0} - f_q}{\tau_q} \tag{3.10}$$

with τ_q the relaxation time and $f_{q,0}$ the equilibrium distribution. The assumption here is that the perturbed distribution function relaxes exponentially to the equilibrium function, with rate τ_q. Before the method of moments is applied to the BTE a few definitions are stated. The first definition gives the carrier density:

$$d_q(\boldsymbol{x}, t) = \int_{\mathbb{R}^3} f_q \mathrm{d}^3 p \tag{3.11}$$

For the free electron density the following notation is used: $d_{-e}(\boldsymbol{x}, t) = n(\boldsymbol{x}, t)$. The notation for the density of holes is $d_e(\boldsymbol{x}, t) = p(\boldsymbol{x}, t)$. The average of a function g is defined as follows:

$$\langle g \rangle = \frac{1}{d_q} \int_{\mathbb{R}^3} g f_q \mathrm{d}^3 p \tag{3.12}$$

Here g can be either a vector function or a scalar function. The current density can be expressed as follows:

$$\boldsymbol{J}_q = q d_q \langle \boldsymbol{v} \rangle \tag{3.13}$$

For the electron current the notation $\boldsymbol{J}_{-e} = \boldsymbol{J}_n$ is used and for the holes $\boldsymbol{J}_{-e} = \boldsymbol{J}_p$ applies. This concludes all the definitions that are used. approximations/assumptions for the derivations of the carrier continuity equations and the drift-diffusion equations are:

1. The energy function of the electrons and holes is approximated by a parabolic function and given by:

$$E = \frac{\hbar^2 k^2}{2m} = \frac{p^2}{2m} = \frac{1}{2} m v^2 \tag{3.14}$$

2. Mass is isotropic and constant

3. The temperature gradient is zero, this can be stated qualitatively as follows: $\nabla T = 0$

4. The force $\boldsymbol{F}$ is independent of particle momentum. This can be stated more generally in vector notation:

$$\nabla_p \cdot \boldsymbol{F} = 0 \tag{3.15}$$

   In other words: the p-divergence of the force must equal zero.

5. The symmetric part of f_q is isotropic:

$$f_{q,S}(\boldsymbol{p}) = f_{q,S}(\|\boldsymbol{p}\|) = f_{q,S}(\sqrt{p_x^2 + p_y^2 + p_z^2}) \tag{3.16}$$

This is a special case of the diffusion approximation. This approximation is valid after $10^{-11}s$ after the entry of the primary electron. The semi-empirical source function models this first $10^{-11}s$ seconds of the processes.

The derivations is placed in the appendix, but the results are: Carrier continuity equations:

$$\frac{\partial n}{\partial t} - \frac{1}{e}\nabla \cdot \boldsymbol{J}_n = -T_n \tag{3.17}$$

$$\frac{\partial p}{\partial t} + \frac{1}{e}\nabla \cdot \boldsymbol{J}_p = -T_p \tag{3.18}$$

Drift-Diffusion equations:

$$\boldsymbol{J}_n = -e\mu_n n\nabla V + eD_n\nabla n \tag{3.19}$$

$$\boldsymbol{J}_p = -e\mu_p p\nabla V - eD_p\nabla p \tag{3.20}$$

Generation and recombination

The information in this section is taken from [2]. In the previous section a derivation of de drift-diffusion model was shown, but the term R was ignored. This term accounts for the implementation Shockley-Read-Hall(SRH) generation/recombination model. In the used implementation only the trapped electrons have to be tracked, because the relevant physics is contained in de following equation:

$$\frac{\partial n_T}{\partial t} = T_n - T_p \tag{3.21}$$

Here T_n consists of an implementation of the electron capture(R_n) and electron emission(G_n). The term T_p consists of the hole capture (R_p) and the hole emission (G_p). In the following let E_c be the energy of the conduction band, E_v the energy of the valence band and E_t be the energy of the trapping site. Now a more elaborate explanation of the generation/recombination processes is given, along with expressions for the average rates of the processes:

1. Electron capture: In this process an electron from the conduction band gets trapped in a trap in the band-gap. Let the energy at the trap be: E_t. The surplus energy of this process is $E_c - E_t$, which is transmitted to a phonon. The average rate for this process is:

$$R_n = \sigma_n v_{th} n\,(N_T - n_T) \tag{3.22}$$

2. Hole capture: In this process an electron in a trapped moves to the valence band and neutralizes a hole. Also a phonon with energy $E_v - E_t$ is produced. The average rate for this process is:

$$R_p = \sigma_p v_{th} p n_T \tag{3.23}$$

3. Hole emission: In this process a hole moves from a neutral trap to the valence band. An electron is left in the trap. The energy $E_t - E_v$ needs to be supplied in this process. The average rate for this process is:

$$G_p = \sigma_p v_{th} n_i \left(N_T - n_T\right) \tag{3.24}$$

4. Electron emission: A trapped electron moves from the trapping site to the conduction band. The energy $E_c - E_t$ needs to be supplied in this process. The average rate for this process is:

$$R_n = \sigma_n v_{th} n_i n_T \tag{3.25}$$

3.2.3 Boundary and initial conditions

The information in this section is taken from [2]. To finish the DDR-model, boundary conditions on V, n, p, $\boldsymbol{J}_n$ and $\boldsymbol{J}_p$ need to be applied. The boundary conditions on V, n and p at the interface between the sample and its holder are either of a Dirichlet-type or of a Neumann-type. The Dirichlet-type boundary condition is to simulate an ohmic contact and the Neumann-type boundary condition to simulate isolation. At the wall of the vacuum chamber the boundary conditions for these three variables can also be of both Dirichlet and Neumann-type. The boundary conditions on $\boldsymbol{J}_n$ and $\boldsymbol{J}_p$ at the sample vacuum interfaces are of a Robin-type. Defining ν as the outward normal vector at the surface of the sample and Σ as either the upper of the lower sample-vacuum interface, the boundary conditions can be stated as follows:

$$-\boldsymbol{J}_n \cdot \nu = \begin{cases} v_e(n - n_i) - \alpha \frac{\partial V^-}{\partial \nu} & \text{if } n > n_i, \\ 0 & \text{otherwise} \end{cases} \tag{3.26}$$

$$-\boldsymbol{J}_p \cdot \nu = 0 \quad \text{On the sample-vacuum interface} \tag{3.27}$$

where

$$\frac{\partial V^-}{\partial \nu}|_\Sigma = \begin{cases} \frac{\partial V}{\partial \nu} & \text{if } \frac{\partial V}{\partial \nu} < 0 \\ 0 & \text{otherwise} \end{cases} \tag{3.28}$$

and

$$\alpha\left(\max\left(V^+\right)\right) = \begin{cases} 0 & \text{if } \max\left(V^+\right) < V_{min} \\ \alpha_{max} \frac{\max(V^+) - V_{min}}{V_{max} - V_{min}} & \text{if } V_{min} \leq \max(V^+) < V_{max} \\ \alpha_{max} & \text{otherwise} \end{cases} \tag{3.29}$$

and

$$V^+|_\Sigma = \begin{cases} V & \text{if } V > 0 \\ 0 & \text{otherwise} \end{cases} \tag{3.30}$$

and

$$\max\left(V^+\right) = \text{Maximum of } \left(V^+|_\Sigma - V_g\right) \tag{3.31}$$

and

$$\alpha_{max} = \frac{v_e \int_{\Sigma(n-n_i)} \mathrm{d}A}{\int_\Sigma \frac{\partial V}{\partial \nu} \mathrm{d}A} \tag{3.32}$$

where V_g is the applied potential at Σ, which in this paper is set to zero. The parameter v_e is called the emission velocity. There is no experimental data to determine this parameter, but its expected value is below that of the thermal velocity. With the term $\alpha \frac{\partial V^-}{\partial \nu}$ in equation 3.27 the tertiary electrons current density is modeled, where α controls the magnitude of the tertiary current density and $\frac{\partial V^-}{\partial \nu}$ controls the spatial distribution. When $\boldsymbol{J}_n \cdot \nu = 0$ there is no net secondary electron yield, so the tertiary electron current cancels out the secondary electron current.

3.2.4 Injection of Primary Electron

Now that the governing equations are derived, a method to inject a primary electron at the surface of a material is needed. This is done by adding a source term to the continuity equation of the density of electrons and holes. In [1] a detailed description of different source terms is given.

3.3 Advantages and Disadvantages of the Two Models

In this section the advantages and the disadvantages of both the Monte Carlo model as the DDR-model are discussed.

3.3.1 Monte Carlo model

The advantages of using the Monte Carlo model to simulate the processes inside a dielectric after an electron falls on its surface and the consecutive secondary electron yield of a the dielectric are:

1. There is no need for any empirical data to start the simulation, since only (well) described physical phenomena need to be modeled in the Monte Carlo approach.

2. The second advantage of the Monte Carlo model is the fact that at any moment the kinetic energy of the electron is known. This makes it possible to know the kinetic energy of the electrons that leave the dielectric at the boundary. Using these facts an energy distribution of an electron can be known.

The disadvantages are:

1. The Monte Carlo method is very computationally demanding. One primary electron creates an enormous amount of secondary electrons inside the material, that all need to be tracked by the Monte-Carlo simulation. This makes it hard to simulate the amount of realizations to derive statistically good yields, with low variances. When the trapping/detrapping mechanism is not turned on the simulations are quite quick.

2. The fact that there is no trapping/detrapping mechanism implemented into the Monte Carlo model, makes for another disadvantage. This leads to

expected yields that are too high and do not match with the experimental data.

3. It is hard to model transient processes with the Monte Carlo Simulation, because to get yields with low variances too many electron paths need to be calculated.

3.3.2 DDR-Model

The advantages of the DDR-Model over the Monte Carlo Model are:

1. It is easier to implement a trapping and de-trapping mechanism for the charge carriers inside a dielectric.
2. The DDR-Model can determine the expected yields quicker than the Monte Carlo model, when a trapping/detrapping mechanism is implemented.
3. An implementation for tertiary electrons is also simple to implement into the boundary conditions.
4. The DDR-Model makes it possible to see the time evolution of the yields.

The disadvantages are:

1. The main disadvantage is the fact that the DDR approach needs a semi-emperical source to start off the simulation. It is not possible for the DDR-model to use the known physical phenomena and implementing this in the first $1 \cdot 10^{-11}$ seconds.
2. The second disadvantage is that the DDR-model does not track the kinetic energy of the charge carriers, but only works with charge densities, in combination with the macroscopic processes: diffusion and drift.
3. Another disadvantage is the need for the DDR-model to tune the emission velocity, capture cross-sections and the density of traps.

3.4 Connection MC-Model and DDR-Model

In this section the connection between the Monte Carlo model and the drift-diffusion model is made. This connection is established by first connecting the MC-model to the BTE. Consequently the connection between the MC-model and the DDR-model, because the DDR-model is a method of solving the BTE.

The clearest connection between the two models is the fact that the kinematics of the boltzmann transport equation and MC-model are both classical. The collisions in the MC-model are modeled directly, while the collision term in the BTE is approximated. The approximation is not valid if the electrons in the material are not thermalized. This is why the semi-emperical source functions models the creation of electron-hole pairs and the transport of electrons and holes during this stage of the processes. The semi-empirical source function is based upon many Monte-Carlo simulations.

Furthermore, if a trapping/detrapping mechanism was build into the MC-model, it would be possible to determine the distribution function, with Monte-Carlo simulations. So under certain conditions/approximations the Monte Carlo is also a solving method for the Boltzmann transport equation.

Chapter 4

Simulations with DDR-model

In this chapter several simulations are presented. All the simulations are done in COMSOL 5.2, with implementations of the DDR-model by Behrouz Raftari. The simulations are done on a rectangular 2D surface, which is then rotated around its left axis to acquire the results for a 3D disk.

4.1 Tuning Parameters

In order to simulate the processes, that lead up to the radiation of electrons from a material, there are a few parameters that need to be tuned to experimental data. The parameters that needed tuning were v_e, the capture cross-sections and the density of traps. These parameters were tuned by Behrouz Raftari such that the standard reflection yield of a bulk sample corresponds to the experimentally measured standard yields. The standard yield is the yield, caused by a single primary electron that falls on the surface of a material. As B. Raftari explains in [2], both the capture cross-sections and the density of traps only influence the shape of the yield-energy curve. When these parameters are increased, the high-energy tail is higher in the yield-energy curve. The emission velocity directly influences the height of the curve. The parameters of the unpolished amorphous alumina are as follows:

ϵ_r	relative permittivity	10
μ_n	Electron mobility	4 $\mathrm{cm^2V^{-1}s^{-1}}$
μ_p	Hole mobility	0.002 $\mathrm{cm^2V^{-1}s^{-1}}$
σ_n	Electron mean trapping cross section	10^{-15} $\mathrm{cm^2}$
σ_p	Hole mean trapping cross section	10^{-17} $\mathrm{cm^2}$
ρ	Density	3.98 $g\mathrm{cm^{-3}}$
E_i	Ionization Energy	28 eV
N_t	Trapping site density	$10^{20}\mathrm{cm^{-3}}$
v_e	Emission velocity	$135\mathrm{cms^{-1}}$

It should also be noted that n_t is the density of trapped electrons and $N_t - n_t = p_t$ is the density of trapped holes.

4.2 Fitting of penetration depth

For electron with a kinetic energy that is higher than 2000eV the penetration depth of an electron with energy E_0 is given in the following empirical formula by Seiler ([1]):

$$R(E_0, \rho) = 115 \frac{E_0^{1,66}}{\rho} [nm] \quad E_0 \geq 2000eV \tag{4.1}$$

with ρ the density of the sample. For energies lower than 2000eV a data set with measured penetration depths for certain primary electron energies is used. To acquire a continuous penetration depth formula for alumina in the entire spectrum of possible primary energies a polynomial fit of order 8 is done. The formula for this fit looks as follows:

$$R(E_0) = p_1 x^8 + p_2 x^7 + p_3 x^6 + p_4 x^5 + p_5 x^4 + p_6 x^3 + p_7 x^2 + p_8 x + p_9 \tag{4.2}$$

The parameters are listed in the table below:

p_1	4.528e-29
p_2	-2.042e-24
p_3	3.854e-20
p_4	-3.959e-16
p_5	2.422e-12
p_6	-9.331e-9
p_7	3.356e-5
p_8	0.001661
p_9	0.02938

It is important to note that this fit is for alumina. For another material a different fit has to be done.

4.3 Single Impact

In this section the results of simulating the electron yield after a single electron falls on the surface of an alumina membrane are presented. For the simulations three different membrane thicnesses are used: 15nm, 20nm and 30nm. Plots of the transmission and reflection yields for unpolished alumina are presented in the figures below. In order to determine how fine the used mesh grid for the

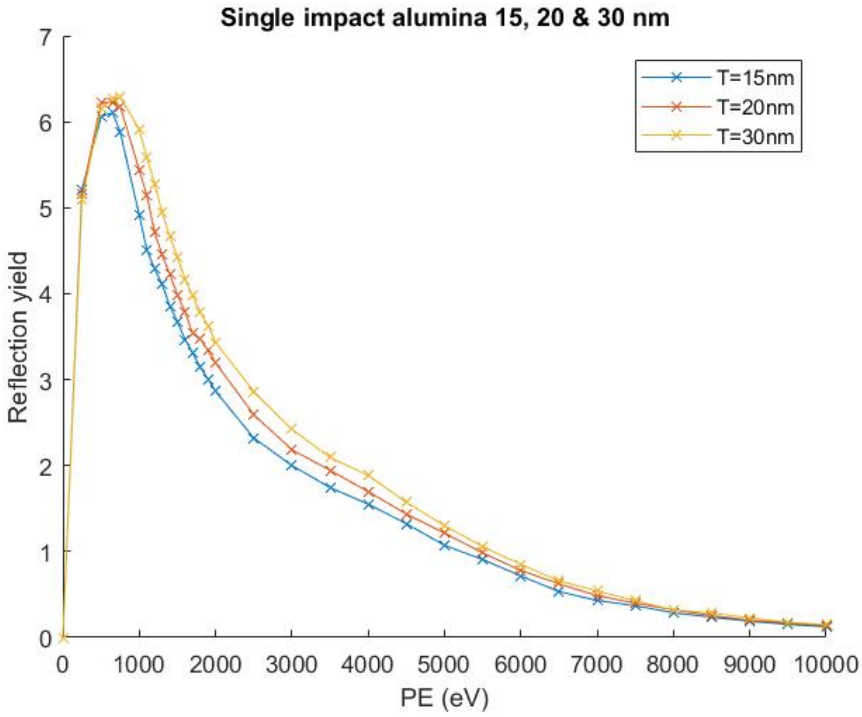

Figure 4.1: This figure shows the reflection yield of an alumina membrane with three different thicknesses. On the x-axis the kinetic energy of the primary electron is displayed.

simulation had to be to acquire accurate results, I first took a maximum length dimension of a grid element at $1.6 \cdot 10^{-16}$. Subsequently an approximately two times finer grid is used. The results are that the difference in secondary electron yield for both grids is about 0.5%. This means that the results are accurate enough with the first grid, however all the single impact simulations are done with the second finer grid.

The curves of the reflection yield are very similar. The maximum variates only very slightly and when the energy increases, the yield goes to 0.

In graph for the transmission yield, it can clearly be seen that when the thickness of the membrane is increased, the maximum transmission yield decreases. Also a higher energy primary electron is needed to get the maximum transmission yield, when the membrane is thicker. The last part resulted in the question

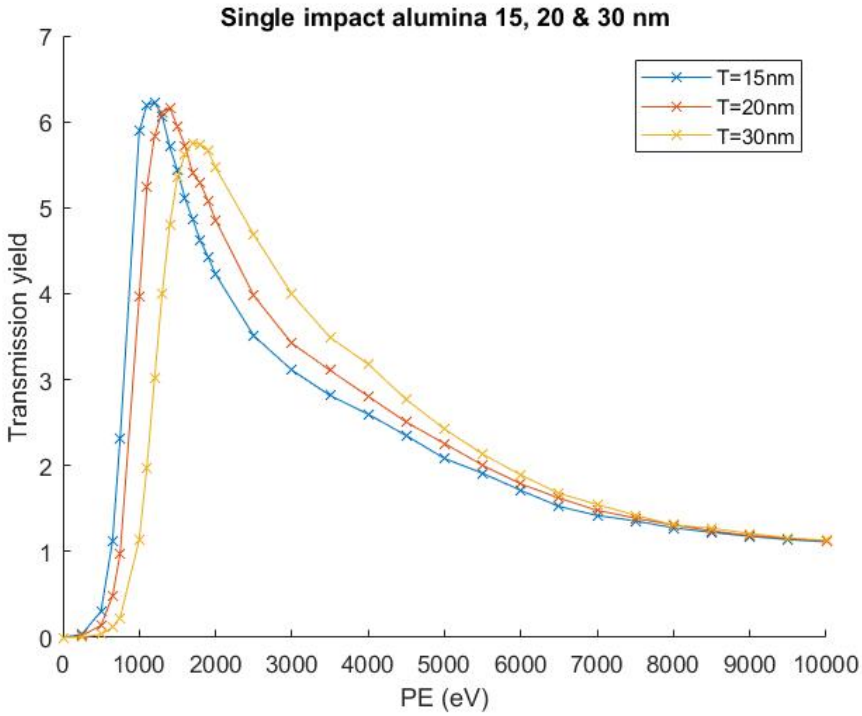

Figure 4.2: This figure shows the transmission yield of an alumina membrane with three different thicknesses. On the x-axis the kinetic energy of the primary electron is displayed.

if it is possible to find the ideal membrane thickness for a given primary energy. This is investigated further below. The maxima of the transmission yield curves from figure 4.2 are shown in the table below:

Thickness (nm)	Primary Energy (eV)	Transmission Yield
15	1200	6.22
20	1400	6.16
30	1700	5.75

4.3.1 Generation Time

It is also interesting to know how the electron yield evolves in time. For this purpose single impact simulations are done with a beam energy of 1000eV and an alumina membrane with thickness 20nm. The definition of t_g is the time it takes to create all the secondary charge carriers inside the material, due to one primary electron impact. It is interesting to note that influence of the generation time on the secondary electron yield is almost nothing. This can be seen in the following table:

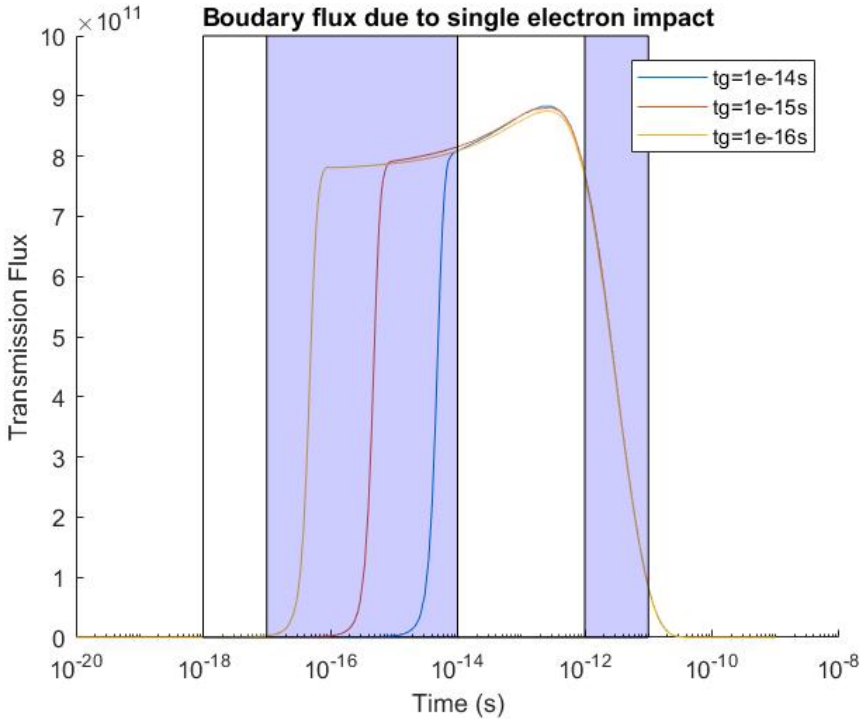

Figure 4.3: In this figure the transmission boundary fluxes over time, after the single impact of a $1keV$ electron, are displayed of three different generation times. The boxes represent the different stages of the processes inside the insulator, which are stated in Chapter 2.

t_g (s)	Reflection Yield	Transmission Yield
$1{\cdot}10^{-14}$	5.4185	3.953464
$1{\cdot}10^{-15}$	5.4036	3.939264
$1{\cdot}10^{-16}$	5.3565	3.908164

The simulated expected yields are all simulated with the same mesh grid. This means that the generation time can be taken as any of the following times: $1 \cdot 10^{-14}s, 1 \cdot 10^{-15}s$ or $1 \cdot 10^{-16}s$. Physically this is understandable because in the first stages the secondary electrons have not had the time to drift/diffuse to the boundary of the sample. So very few particles satisfy the conditions to leave the sample after just $10^{-16}s$.

4.3.2 Thickness Dependence

In this section the possibility is investigated that for a given primary energy, the thickness which gives the highest secondary transmission yield, is a constant times the penetration depth. In formula form this looks as follows:

$$T = aR \tag{4.3}$$

where T is the membrane thickness, R is the penetration depth and a is a yet to be determined constant. To determine the constant a two beam energies

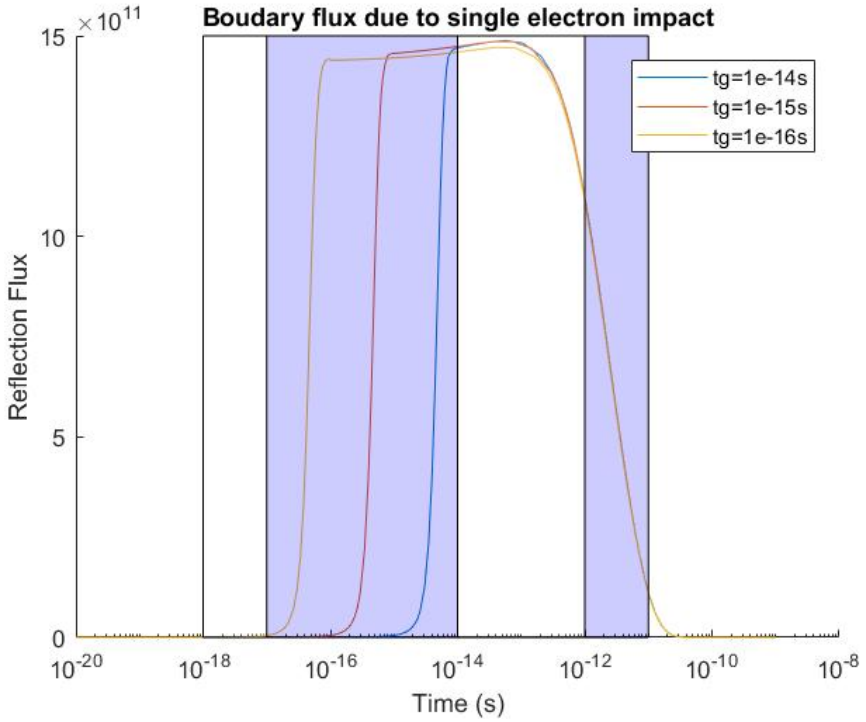

Figure 4.4: In this figure the reflection boundary fluxes over time, after the single impact of a $1keV$ electron, are displayed of three different generation times. The boxes represent the different stages of the processes inside the insulator, which are stated in Chapter 2.

are tested: $1000eV$ and $2500eV$. For each primary energy the transmission yield for a range of thicknesses between $0.2R$ and $0.6R$ shall be determined in a simulation. Here R corresponds to the (theoretical) penetration depth of a primary electron with energy E_0. The results are stated below. The first tabular are the results with primary beam energy $1000eV$ and the second tabular are the results with a beam energy of $2500eV$.

T	a	Transmission Yield
8.4	0.3	5.504
9.8	0.35	5.995
11.2	0.4	6.220
12.6	0.45	6.267
14	0.5	6.117
15.4	0.55	5.774
16.8	0.6	5.299

In the table for $1000eV$ it is clear that at $0.45R$ is the optimal thickness, which give the maximum transmission yield. Now the results for $2500eV$ are presented:

T	a	Transmission Yield
39.67	0.3	5.065
46.29	0.35	5.161
52.90	0.4	4.947
59.51	0.45	4.728
66.12	0.5	4.346
72.74	0.55	3.793
79.35	0.6	3.230

From these two tables it becomes clear that a cannot be a constant, because the optimal thickness for a primary beam with energy $2500eV$ lies at $0.35R$. This conclusion does not mean that there is not a function of primary energy, that gives the membrane thickness that will give the maximum transmission yield, but this option is not further investigated in this paper.

4.4 Electron Bombardement

In this section the results of electron bombardment of a thin membrane of unpolished amorphous alumina are presented and discussed. In the simulations the electrons land on the same spot of the sample every time, so the results presented here are a worst case scenario. In these figures the general rule of

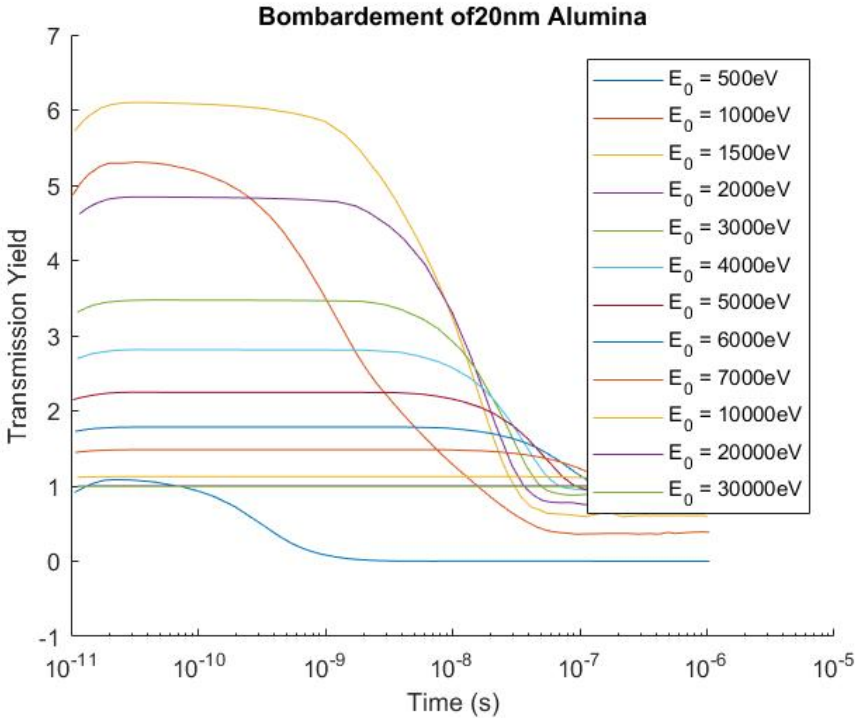

Figure 4.5: Here the electron yield over time of bombardment of unpolished amorphous alumina for different primary electron energies are shown. The current of the primary electron beam is 100 pA.

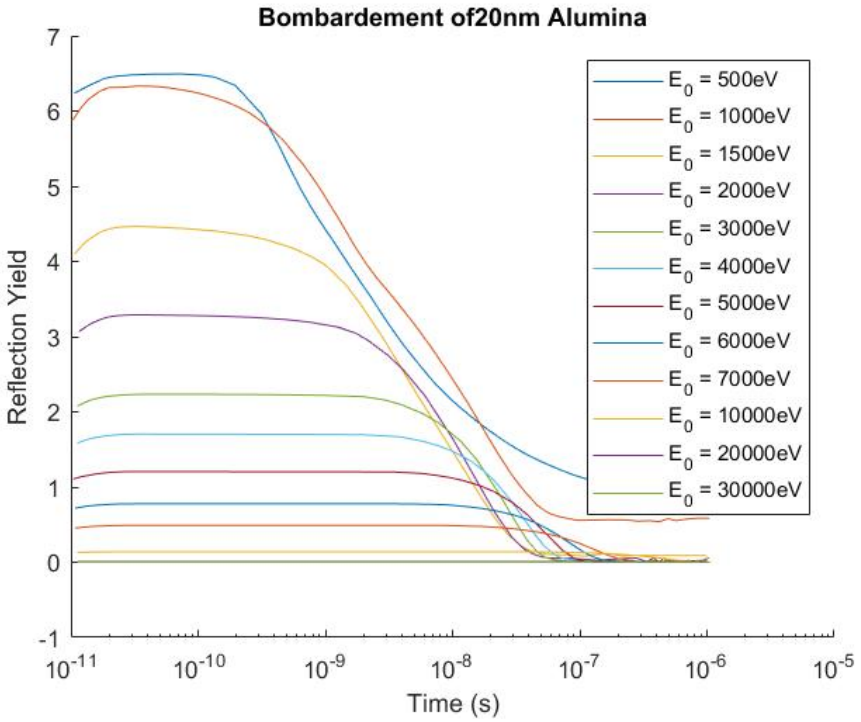

Figure 4.6: Here the electron yield over time of bombardment of unpolished amorphous alumina for different primary electron energies are shown. The current of the primary electron beam is 100 pA.

thumb can be acquired that the higher the beam energy the sooner the secondary electron yields drops. It is interesting to determine how many electrons have to fall at the surface of the sample to get half the standard transmission yield. For the beam with primary energy $1500eV$ the time it takes to get half the transmission yield is about $10^{-8}s$. The beam current is $100pA$. This means that $100pA \cdot 10^{-8}s = 1 \cdot 10^{-18}C$. Dividing this by elementary electron charge the result is approximately 10 electrons. So when 10 electrons have fallen in the same spot it only takes 10 electrons with primary energy $1500eV$ to decrease the yield by a factor 2.

4.5 Charging

In this section charging phenomena due to trapped charges are investigated. First this is done by looking at the trapped charge densities on the surface of a 20nm membrane after a single impact simulation. This is done with primary energies $1000eV$ and $2500eV$. The second investigation is done, after a simulation of a sustained bombardment.

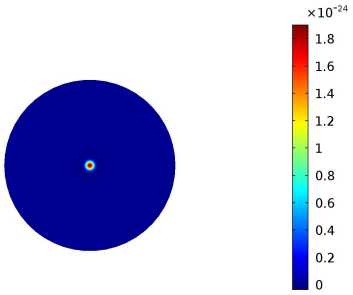

(a) Primary energy of 1000eV.

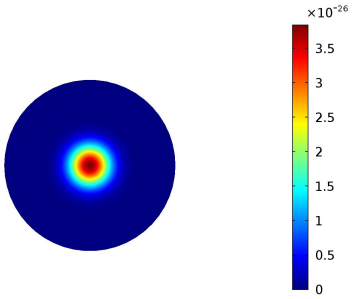

(b) Primary energy of 2500eV.

Figure 4.7: In this figure the trapped charge density p_t, of the top surface of a 20nm membrane is given, after a single impact simulation.

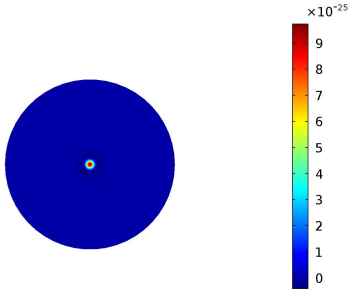

(a) Primary energy of 1000eV.

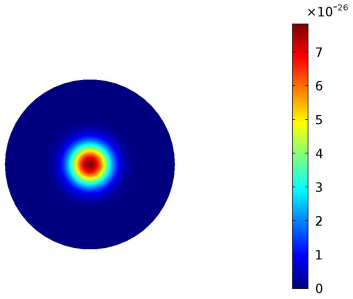

(b) Primary energy of 2500eV.

Figure 4.8: In this figure the trapped charge density p_t, of the bottom surface of a 20nm membrane is given, after a single impact simulation.

4.5.1 Single Impact

In the figures below it is clear that a higher primary energy leaves a larger part of the surface layer with trapped charges. The figures show the surfaces a nanosecond after the primary electron has impacted. The fact that the density is positive means that there are trapped holes at both surfaces. So when a second primary electron falls on the top surface it would actually accelerate toward the surface.

4.5.2 Bombardment

In this section the distribution of trapped charges after a sustained electron bombardment in a single spot is shown. In the previous section about electron bombardment it was shown that the yields quickly diminished, this is because the local potential at the surface of the thin membrane, becomes too high for secondary electrons to escape. The trapped holes pull the secondary electrons back into the membrane. The maximum potential at the boundary is set to 10V, this is because the secondary electrons have an energy between 0-10eV. So when the maximum potential is reached, no electrons can leave.

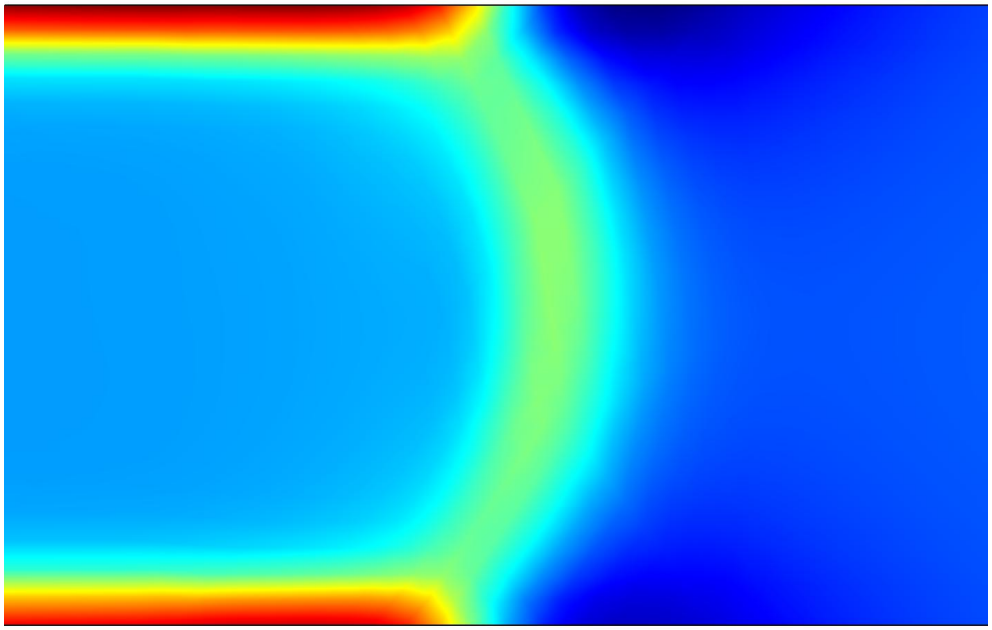

Figure 4.9: In this figure the trapped charge density p_t, in a 20nm alumina membrane is shown, after sustained electron bombardment, with a primary energy of 1000eV and a current of 100pA.

The legend of figures 4.9 and 4.10 is the same. In figure 4.10 we see that the area of the trapped holes is bigger than that of the top surface of an alumina sample after single impact, which was discussed in the previous paragraph. Negative charge density, as is indicated in the legend, represent trapped holes. The images are both showing the trapped charge density after electron bombardment of $1\mu s$.

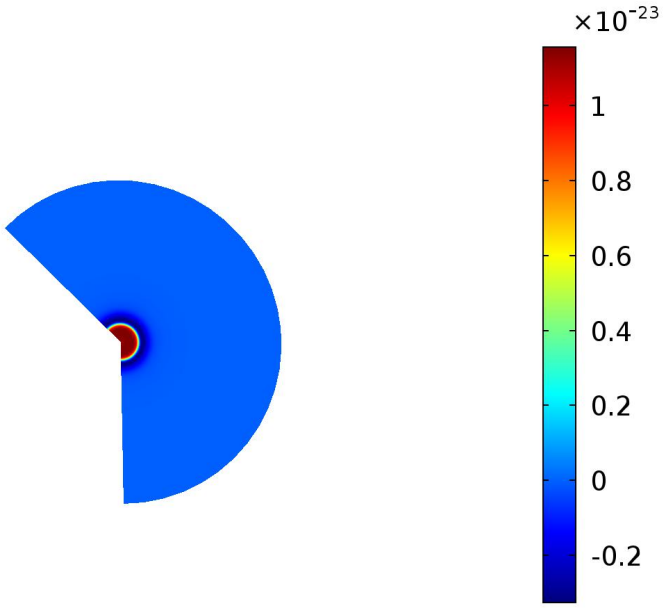

Figure 4.10: In this figure the top view of a 20nm alumina membrane is shown, after 1 microsecond of electron bombardment, with a primary energy of 1000eV and a current of 100pA. Positive charge density represents the density of trapped holes p_t.

4.5.3 Electron inflow

The last simulation is a simulation with electron inflow at the boundary. In this simulation a layer of 5nm alumina is placed on top of a 15nm layer alumina. The boundary conditions for the lower 15nm layer are the same as for the isolated case, but at the boundary of the 5nm layer charge density is kept at the intrinsic charge density. The result is shown in figure 4.11, where it is also compared to the isolated case. For the case with electron inflow it can be seen that it takes longer for the secondary electron yield to drop. It also seems to recover some of the secondary electron yield after $10^{-5}s$. The yield at the end for the case with inflow of electrons is 1.5, while the yield for the isolated case is about 0.8. This is a significant increase. Due to computational problems it was not possible to place a more conducting material on top of the 15nm alumina, but it could be expected that the yield might increase even more when this is the case.

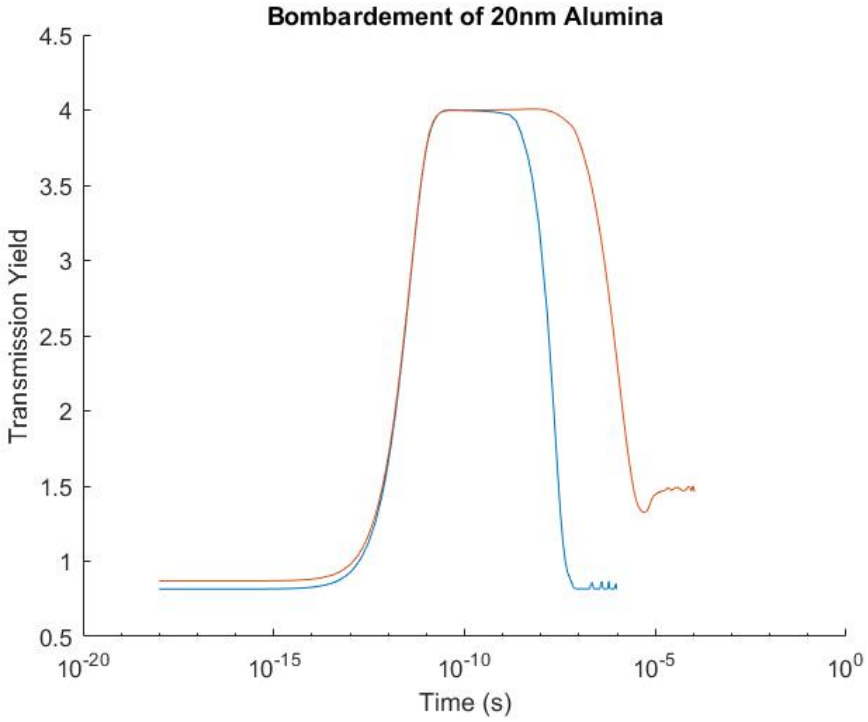

Figure 4.11: In this figure the the secondary transmission yield of a isolated sample and a sample where electron inflow from the upper boundary is allowed.

Chapter 5

Conclusions

In conclusion we can say that both the Monte Carlo model and the DDR model may be viewed as different solution methods of the Boltzmann transport equation. The strengths of the Monte Carlo model are that it does not use empirical data and that an energy spectrum of the secondary electrons can be found. Its weaknesses are that it is harder to implement a trapping/detrapping mechanism, it becomes very computationally demanding when all the processes are accounted for and the time-evolution of the yield is not known. The main advantages of the DDR model are that it can model transient processes, a trapping/detrapping model is easier to implement, tertiary electrons can be accounted for. Its disadvantages are: the DDR model needs a semi-empirical source function to start the simulation, the kinetic energy of the particles is not tracked and some parameters need to be tuned.

There are a few main conclusions that we can draw from the simulations on a thin membrane of alumina. We can conclude that charging causes degradation of yield over time. Also the yield may recover if the membrane is grounded. Further work may include simulation of TiN membrane cover and analysis of shocks.

This can be divided into conclusions about single impact of a primary electron, electron bombardment of a thin alumina membrane and electron bombardment with the inflow of electrons at the boundary.

From the simulations with a single primary electron impact, we can conclude that for a membrane of 15nm we get the highest transmission yield of 6.22, which is achieved with a primary electron of 1200eV. The peak yields of the thicker membranes decrease and the primary energy that is needed to achieve the higher secondary electron yield is higher. For 20nm and 30nm, the peak secondary transmission yields are respectively 6.16 and 5.75 at primary energies 1400eV and 1700eV.

From the electron bombardment simulations on an isolated membrane in which all the electrons fall on the same spot, we can conclude that after about 10 electrons falling on the surface of our membrane the transmission secondary electrons are halve that of the yields of a single electron impact.

Bibliography

[1] B. Raftari, N.V. Budko and C. Vuik, *Self-consistent drift-diffusion-reaction model for the electron beam interaction with dielectric samples*, Journal of Applied Physics, TU Delft, 5 November 2015

[2] B. Raftari, N.V. Budko and C. Vuik, *A Modified and Calibrated Drift-Diffusion-Reaction Model for Time-Domain Analysis of Charging Phenomena in Electron-Beam Irradiated Insulators*, Materials Science, TU Delft, 6 Jul 2017

[3] D.I. Vaisburd and K.E. Evdokimov, *The Poole-Frenkel Effect in a dielectric under nanosecond irradiation by an alectron beam with moderate or high current density*, Russian Physics Journal, Vol. 51, No. 12, 2008,Tomsk Polytechnic University

[4] Markus Gritsch, *Numerical Modeling of Silicon-on-Insulator MOSFETs*, Phd Thesis, November 2002, TU Wien

Appendix A

Derivation of the Drift-Diffusion Reaction model from the Boltzmann Transport Equation

In this appendix the derivation of the carrier continuity eqution and the drift-diffusion equations is given. The following list of (nabla) identities is used:

1. $\boldsymbol{A} \cdot \nabla a = \nabla \cdot (a\boldsymbol{A}) - a\nabla \cdot \boldsymbol{A}$
2. $\boldsymbol{B}\nabla \cdot (a\boldsymbol{A}) = \nabla \cdot (a\boldsymbol{A}\boldsymbol{B}) - (a\boldsymbol{A} \cdot \nabla)\,\boldsymbol{B}$
3. $(a\boldsymbol{A} \cdot \nabla)\,\boldsymbol{B} = \nabla \cdot (a\boldsymbol{A}\boldsymbol{B}) - \boldsymbol{B}\nabla \cdot (a\boldsymbol{A})$

When a certain identity is used the number of the identity will placed above the equality sign.

A.1 Carrier continuity equations

To derive the carrier continuity equations with the method of moments the weight function with value 1 is used. This yields:

$$\int_{\mathbb{R}^3} \frac{\partial f_q}{\partial t} \mathrm{d}^3p + \int_{\mathbb{R}^3} (\boldsymbol{F} \cdot \nabla_p f_q)\,\mathrm{d}^3p + \int_{\mathbb{R}^3} \boldsymbol{v} \cdot \nabla f_q \mathrm{d}^3p = \int_{\mathbb{R}^3} \frac{f_{q,0} - f}{\tau_q} \mathrm{d}^3p - T_q \quad \text{(A.1)}$$

With,

$$T_q = \int_{\mathbb{R}^3} \mathcal{T}(f_q) \mathrm{d}^3p \quad \text{(A.2)}$$

This equation will be reviewed term-by-term:

1. Using the definition of $n(\boldsymbol{x}, t)$, the first term becomes:

$$\int_{\mathbb{R}^3} \frac{\partial f_q}{\partial t} \mathrm{d}^3p = \frac{\partial}{\partial t} \int_{\mathbb{R}^3} f_q \mathrm{d}^3p = \frac{\partial d_q(\boldsymbol{x}, t)}{\partial t} \quad \text{(A.3)}$$

2. f_q is finite, so at the boundaries of $\mathbb{R}^3$, $f_q = 0$. Using the divergence theorem and the fact that the p-divergence of the force is zero, the second term becomes:

$$\int_{\mathbb{R}^3} \boldsymbol{F} \cdot \nabla_p f_q \mathrm{d}^3 p \overset{(1)}{=} \int_{\mathbb{R}^3} \nabla_p \cdot (f_q \boldsymbol{F}) \, \mathrm{d}^3 p - \int_{\mathbb{R}^3} f_q \left(\nabla_p \cdot \boldsymbol{F}\right) \mathrm{d}^3 p \tag{A.4}$$

$$= 0 \tag{A.5}$$

3. The divergence of velocity is zero ($\boldsymbol{v}$ is only dependent on the momentum phase variables), quantitatively described with $\nabla \cdot \boldsymbol{v} = 0$. The third term becomes:

$$\int_{\mathbb{R}^3} \boldsymbol{v} \cdot \nabla f_q \mathrm{d}^3 p \overset{(1)}{=} \int_{\mathbb{R}^3} \nabla \cdot (\boldsymbol{v} f_q) \, \mathrm{d}^3 p - \int_{\mathbb{R}^3} f_q \left(\nabla \cdot \boldsymbol{v}\right) \mathrm{d}^3 p \tag{A.6}$$

$$= \nabla \cdot \int_{\mathbb{R}^3} \boldsymbol{v} f_q \mathrm{d}^3 p - 0 \tag{A.7}$$

$$= \nabla \cdot \left(d_q \left\langle \boldsymbol{v} \right\rangle\right) \tag{A.8}$$

4. Both distributions only differ in momentum space and the number of particles does not change. This means that $d_q(\boldsymbol{r}, t) = \langle 1 \rangle = \langle 1 \rangle_0 = d_{q,0}(\boldsymbol{r}, t)$, with $\langle 1 \rangle_0 = \int_{\mathbb{R}^3} f_{q,0} \mathrm{d}^3 p$. The fourth term becomes:

$$\int_{\mathbb{R}^3} \frac{f_{q,0} - f_q}{\tau_q} \mathrm{d}^3 p = 0 \tag{A.9}$$

By combining the results of the term-by-term analysis, the carrier continuity equation becomes:

$$\frac{\partial d_q}{\partial t} + \nabla \cdot \left(d_q \left\langle \boldsymbol{v} \right\rangle\right) = \frac{\partial d_q(\boldsymbol{x}, t)}{\partial t} + \frac{1}{q} \nabla \cdot \boldsymbol{J}_q = -T_q \tag{A.10}$$

The carrier continuity equation for the electrons and holes are:

$$\frac{\partial n}{\partial t} - \frac{1}{e} \nabla \cdot \boldsymbol{J}_n = -T_n \tag{A.11}$$

$$\frac{\partial p}{\partial t} + \frac{1}{e} \nabla \cdot \boldsymbol{J}_p = -T_p \tag{A.12}$$

where $\boldsymbol{J}_n$ and $\boldsymbol{J}_p$ are the electron and hole current density, respectively.

A.2 Drift-Diffusion

To derive the drift-diffusion equations with the method of moments the weight function $\boldsymbol{v}$ is used. This yields:

$$\int_{\mathbb{R}^3} \boldsymbol{v} \frac{\partial f_q}{\partial t} \mathrm{d}^3 p + \int_{\mathbb{R}^3} \boldsymbol{v} \left(\boldsymbol{F} \cdot \nabla_p f_q\right) \mathrm{d}^3 p + \int_{\mathbb{R}^3} \boldsymbol{v} \left(\boldsymbol{v} \cdot \nabla f_q\right) \mathrm{d}^3 p = \int_{\mathbb{R}^3} \boldsymbol{v} \frac{f_{q,0} - f_q}{\tau_q} \mathrm{d}^3 p - \int_{\mathbb{R}^3} \boldsymbol{v} \mathcal{T}(f_q) \mathrm{d}^3 p \tag{A.13}$$

This equation is be reviewed term-by-term:

1. The partial derivative in time of the group velocity is zero, so with the definition of the average, the first term becomes:

$$\int_{\mathbb{R}^3} \boldsymbol{v} \frac{\partial f_q}{\partial t} \mathrm{d}^3 p = \frac{\partial}{\partial t} \int_{\mathbb{R}^3} \boldsymbol{v} f_q \mathrm{d}^3 p = \frac{\partial \left(d_q \left\langle \boldsymbol{v} \right\rangle \right)}{\partial t} \tag{A.14}$$

2. First the fact that $\nabla_p \cdot \boldsymbol{F} = 0$ is used, then the divergence theorem is applied. Because f is finite, the surface integral becomes zero. The second term becomes:

$$\begin{aligned}
\int_{\mathbb{R}^3} \boldsymbol{v} \left(\boldsymbol{F} \cdot \nabla_p f_q \right) \mathrm{d}^3 p &\overset{(1)}{=} \int_{\mathbb{R}^3} \boldsymbol{v} \left(\nabla_p \cdot f_q \boldsymbol{F} \right) \mathrm{d}^3 p - \int_{\mathbb{R}^3} f_q \boldsymbol{v} \left(\nabla_p \cdot \boldsymbol{F} \right) \mathrm{d}^3 p \\
&\overset{(3)}{=} \int_{\mathbb{R}^3} \nabla_p \cdot \left(f_q \boldsymbol{v} \boldsymbol{F} \right) \mathrm{d}^3 p - \int_{\mathbb{R}^3} \left(f_q \boldsymbol{F} \cdot \nabla_p \right) \boldsymbol{v} \mathrm{d}^3 p - 0 \\
&= 0 - \int_{\mathbb{R}^3} \left(\frac{f_q \boldsymbol{F}}{m} \right) \mathrm{d}^3 p \\
&= -\frac{\boldsymbol{F}}{m} \int_{\mathbb{R}^3} f_q \mathrm{d}^3 p \\
&= -\frac{q \boldsymbol{E}}{m} d_q(\boldsymbol{x}, t)
\end{aligned} \tag{A.15}$$

3. The following identities: $\nabla \boldsymbol{v} = \boldsymbol{0}$ and $\nabla \cdot \boldsymbol{v} = 0$ are true because $\boldsymbol{v} = \frac{\boldsymbol{p}}{m}$. The third term becomes:

$$\begin{aligned}
\int_{\mathbb{R}^3} \boldsymbol{v} \left(\boldsymbol{v} \cdot \nabla f_q \right) \mathrm{d}^3 p &\overset{(1)}{=} \int_{\mathbb{R}^3} \boldsymbol{v} \nabla \cdot \left(f_q \boldsymbol{v} \right) \mathrm{d}^3 p - \int_{\mathbb{R}^3} \boldsymbol{v} f_q \left(\nabla \cdot \boldsymbol{v} \right) \mathrm{d}^3 p \\
&\overset{(2)}{=} \int_{\mathbb{R}^3} \nabla \cdot \left(f_q \boldsymbol{v} \boldsymbol{v} \right) \mathrm{d}^3 p - \int_{\mathbb{R}^3} \left(f_q \boldsymbol{v} \cdot \nabla \right) \boldsymbol{v} \mathrm{d}^3 p - 0 \\
&= \int_{\mathbb{R}^3} \nabla \cdot \left(f_q \boldsymbol{v} \boldsymbol{v} \right) \mathrm{d}^3 p
\end{aligned}$$

4. The fourth term becomes:

$$\int_{\mathbb{R}^3} \boldsymbol{v} \frac{f_{q,0} - f_q}{\tau_q} \mathrm{d}^3 p = d_q \frac{\left\langle \boldsymbol{v}_0 \right\rangle - \left\langle \boldsymbol{v} \right\rangle}{\tau_q} = -\frac{d_q \left\langle \boldsymbol{v} \right\rangle}{\tau_q} \tag{A.16}$$

   With,

$$\left\langle \boldsymbol{v}_0 \right\rangle = \int_{\mathbb{R}^3} \boldsymbol{v} f_{q,0} \mathrm{d}^3 p = 0 \tag{A.17}$$

   This equality is true, because the average velocity at equilibrium is zero.

5. The generation/recombination process is independent of the momentum phase space. The fifth term becomes:

$$\int_{\mathbb{R}^3} \boldsymbol{v} \mathcal{T}(f_q) \mathrm{d}^3 p = \mathcal{T}(f_q) \int_{\mathbb{R}^3} \boldsymbol{v} \mathrm{d}^3 p = 0 \tag{A.18}$$

After combining the term-by-term analysis equation $A.13$ becomes:

$$\frac{\partial \left(d_q \left\langle \boldsymbol{v} \right\rangle \right)}{\partial t} - \frac{q \boldsymbol{E}}{m} d_q + \int_{\mathbb{R}^3} \nabla \cdot \left(f_q \boldsymbol{v} \boldsymbol{v} \right) \mathrm{d}^3 p = -\frac{d_q \left\langle \boldsymbol{v} \right\rangle}{\tau}$$

Now only:

$$\int_{\mathbb{R}^3} \nabla \cdot (f_q \boldsymbol{v}\boldsymbol{v}) \, \mathrm{d}^3 p = \nabla \cdot \int_{\mathbb{R}^3} (f_q \boldsymbol{v}\boldsymbol{v}) \, \mathrm{d}^3 p \tag{A.19}$$

needs to be worked out. First f_q is split in a symmetric part and an anti-symmetric part:

$$f_q(\boldsymbol{p}) = f_{q,S}(\boldsymbol{p}) + f_{q,A}(\boldsymbol{p}) \tag{A.20}$$

Now the integral over the anti-symmetric part cancels to zero, because $\boldsymbol{v}\boldsymbol{v}$ is symmetric in $\boldsymbol{p}$. The assumption that the symmetric part of f is isotropic is now applied in the integral:

$$\nabla \cdot \int_{\mathbb{R}^3} (f_q \boldsymbol{v}\boldsymbol{v}) \, \mathrm{d}^3 p = \nabla \cdot \int_{\mathbb{R}^3} (f_{q,S}(\boldsymbol{p}) \boldsymbol{v}\boldsymbol{v}) \, \mathrm{d}^3 p \tag{A.21}$$

Because $f_{q,S}(\boldsymbol{p})$ is symmetric in the three momentum phase variables, the following identity applies:

$$\int_{\mathbb{R}} v_l f_S(\|p\|) \mathrm{d}p_l = \int_{\mathbb{R}} \frac{p_l}{m} f_S(\|p\|) \mathrm{d}p_l = 0 \tag{A.22}$$

for $l = x, y, z$. This leaves only the integrals on the diagonal:

$$\langle v_l \rangle = \frac{1}{m^2} \int_{\mathbb{R}^3} p_l^2 f_{q,S}(\sqrt{p_x^2 + p_y^2 + p_z^2}) \mathrm{d}p_l = A \tag{A.23}$$

For some A and $l = x, y, z$. This means that:

$$\left\langle v_x^2 \right\rangle = \left\langle v_y^2 \right\rangle = \left\langle v_z^2 \right\rangle = A \tag{A.24}$$

Writing this in the following form yields:

$$3A = \left\langle v_x^2 \right\rangle + \left\langle v_y^2 \right\rangle + \left\langle v_z^2 \right\rangle = \left\langle v_x^2 + v_y^2 + v_z^2 \right\rangle = \left\langle v^2 \right\rangle \tag{A.25}$$

So the following relation is obtained:

$$A = \frac{\left\langle v^2 \right\rangle}{3} = \frac{2}{3m} \langle E \rangle \tag{A.26}$$

In the last equality the relation $E_{kin} = \frac{1}{2} m v^2$ is used. Now, the derived expressions can finally be combined and the integral expressed in n. To do this the relation $\langle E \rangle = \frac{3}{2} k_B T$ is also used. This last expression will be derived in the

section named closure. The integral becomes:

$$\int_{\mathbb{R}^3} \nabla \cdot (f_q \boldsymbol{v}\boldsymbol{v}) \, \mathrm{d}^3 p = \int_{\mathbb{R}^3} \nabla \cdot f_q \begin{pmatrix} v_x^2 & v_x v_y & v_x v_z \\ v_y v_x & v_y^2 & v_y v_z \\ v_z v_x & v_y v_z & v_z^2 \end{pmatrix} \mathrm{d}^3 p \tag{A.27}$$

$$= \nabla \cdot \begin{pmatrix} \int v_x^2 f_q \mathrm{d}^3 p & \int v_x v_y f_q \mathrm{d}^3 p & \int v_x v_z f_q \mathrm{d}^3 p \\ \int v_y v_x f_q \mathrm{d}^3 p & \int v_y^2 f_q \mathrm{d}^3 p & \int v_y v_z f_q \mathrm{d}^3 p \\ \int v_z v_x f_q \mathrm{d}^3 p & \int v_y v_z f_q \mathrm{d}^3 p & \int v_z^2 f_q \mathrm{d}^3 p \end{pmatrix} \tag{A.28}$$

$$= \nabla \cdot \begin{pmatrix} d_q \left\langle v_x^2 \right\rangle & 0 & 0 \\ 0 & d_q \left\langle v_y^2 \right\rangle & 0 \\ 0 & 0 & d_q \left\langle v_z^2 \right\rangle \end{pmatrix} \tag{A.29}$$

$$= \begin{pmatrix} \frac{\partial d_q \left\langle v_x^2 \right\rangle}{\partial x} & \frac{\partial d_q \left\langle v_y^2 \right\rangle}{\partial y} & \frac{\partial d_q \left\langle v_z^2 \right\rangle}{\partial z} \end{pmatrix}^T \tag{A.30}$$

$$= \frac{1}{3} \begin{pmatrix} \frac{\partial d_q \left\langle v^2 \right\rangle}{\partial x} & \frac{\partial d_q \left\langle v^2 \right\rangle}{\partial y} & \frac{\partial d_q \left\langle v^2 \right\rangle}{\partial z} \end{pmatrix}^T \tag{A.31}$$

$$= \frac{1}{3} \nabla \left(n \left\langle v^2 \right\rangle \right) \tag{A.32}$$

$$= \frac{2}{3m} \nabla \left(n \left\langle E \right\rangle \right) \tag{A.33}$$

$$= \frac{k_B T}{m} \nabla n \tag{A.34}$$

Combining all the results, the drift-diffusion becomes:

$$\frac{d_q \left\langle \boldsymbol{v} \right\rangle}{\tau_q} + \frac{\partial \left(d_q \left\langle \boldsymbol{v} \right\rangle \right)}{\partial t} = \frac{q\boldsymbol{E}}{m} d_q - \frac{k_B T}{m} \nabla d_q \tag{A.35}$$

Multiplying by $q\tau$, the equation becomes:

$$q d_q \left\langle \boldsymbol{v} \right\rangle + \tau_q \frac{\partial \left(q d_q \left\langle \boldsymbol{v} \right\rangle \right)}{\partial t} = \frac{q^2 \tau_q \boldsymbol{E}}{m} d_q - \frac{q\tau_q}{m} k_B T \nabla d_q \tag{A.36}$$

Now a few substitutions are made:

$$\boldsymbol{J}_q = q d_q \left\langle \boldsymbol{v} \right\rangle \tag{A.37}$$

$$\mu_q = \frac{e\tau_q}{m} \qquad \text{(Mobility)} \tag{A.38}$$

$$D_q = \frac{\mu_q k_B T}{e} \quad \text{(Diffusion constant, Einstein relation)} \tag{A.39}$$

Also in an insulator, $\tau \sim 10^{-15}$ for electrons and $\tau \sim 10^{-18}$ for holes. This means that the approximation: $\tau \frac{\partial \boldsymbol{J}_n}{\partial t} \approx 0$ is valid. This yields:

$$\boldsymbol{J}_q = e\mu n \boldsymbol{E} - qD \nabla d_q \tag{A.40}$$

The drift-diffusion equations for electrons and holes are:

$$\boldsymbol{J}_n = e\mu_n n \boldsymbol{E} + eD_n \nabla n \tag{A.41}$$

$$\boldsymbol{J}_p = e\mu_p p \boldsymbol{E} - eD_p \nabla p \tag{A.42}$$

with μ_n and μ_p the mobility of the electrons and holes, respectively and D_n and D_p the diffusion constants of the electrons and holes. To connect these equations to Poisson's equation the electric field is written in its potential form: $\boldsymbol{E} = -\nabla V$. The drift-diffusion equations become:

$$\boldsymbol{J}_n = -e\mu_n n\nabla V + eD_n\nabla n \tag{A.43}$$
$$\boldsymbol{J}_p = -e\mu_p p\nabla V - eD_p\nabla p \tag{A.44}$$

A.3 Closure

In this section a derivation for the expression $\langle E\rangle$ is given. Two major assumptions have to be made here. The first assumption is that (the symmetric part of) f is a Maxwellian distribution of the form:

$$f = A\exp(-\frac{E}{k_BT}) \tag{A.45}$$

A discussion about the validity of this assumption can be found in reference [4]. The second assumption is that the energy oth the carrier is the parabolic dispersion relation:

$$E = \frac{\hbar^2k^2}{2m} = \frac{p^2}{2m} \tag{A.46}$$

Now the expression for $n\langle E\rangle$ will be derived:

$$n\langle E\rangle = \int_{\mathbb{R}^3} Ef\mathrm{d}^3p = \int_{\mathbb{R}^3} EA\exp\left(-\frac{E}{k_BT}\right)\mathrm{d}^3p \tag{A.47}$$

Now a coordinate change from Cartesian to spherical coordinates is made:

$$n\langle E\rangle = \int_0^\infty 4\pi p^2EA\exp\left(-\frac{E}{k_BT}\right)\mathrm{d}p \tag{A.48}$$

The parabolic dispersion relation provides the following relation: $\mathrm{d}p = \frac{m}{p}\mathrm{d}E$. This means:

$$n\langle E\rangle = 4\pi mA\int_0^\infty pE\exp\left(-\frac{E}{k_BT}\right)\mathrm{d}E \tag{A.49}$$

Now the substitution $p = \sqrt{2mE}$ is made:

$$n\langle E\rangle = 2\pi\left(2m\right)^{3/2}A\int_0^\infty E^{3/2}\exp\left(-\frac{E}{k_BT}\right)\mathrm{d}E \tag{A.50}$$

The last substitution that is needed is $u = \frac{E}{k_BT}$. This substitution gives rise to the relation between the differentials: $\mathrm{d}E = k_BT\mathrm{d}u$:

$$n\langle E\rangle = 2\pi\left(2mk_BT\right)^{3/2}k_BTA\int_0^\infty u^{3/2}\exp\left(-u\right)\mathrm{d}u \tag{A.51}$$
$$= 2\pi\left(2mk_BT\right)^{3/2}k_BTA\Gamma\left(\frac{5}{2}\right) \tag{A.52}$$
$$= \frac{3}{2}\left(2m\pi k_BT\right)^{3/2}k_BTA \tag{A.53}$$

The expression for A can be obtained by normalizing f:

$$n = \int_{\mathbb{R}^3} f \mathrm{d}^3 p \tag{A.54}$$

To calculate this integral a coordinate change to spherical coordinates is made again. Also the same substitution $u = \frac{E}{k_B T}$ is made. This yields:

$$\begin{aligned} n &= \int_{\mathbb{R}^3} A \exp\left(-\frac{E}{k_B T}\right) \mathrm{d}^3 p \\ &= 4\pi A \int_0^\infty p^2 \exp\left(-\frac{E}{k_B T}\right) \mathrm{d}p \\ &= 8\pi A m k_B T \sqrt{\frac{m k_B T}{2}} \int_0^\infty u^{1/2} \exp\left(-u\right) \mathrm{d}u \\ &= 2\pi A \left(2 m k_B T\right)^{3/2} \Gamma\left(\frac{3}{2}\right) \\ &= A \left(2 m \pi k_B T\right)^{3/2} \end{aligned} \tag{A.55}$$

This means that the normalization constant A is:

$$A = n \left(2 m \pi k_B T\right)^{-3/2} \tag{A.56}$$

This yields:

$$\langle E \rangle = \frac{3}{2} k_B T \tag{A.57}$$

Appendix B

Poisson's equation

First of all Maxwell's equations will be stated (ϵ is considerd a constant, for an isotropic, permeable and conducting semiconductor):

$$\boldsymbol{\nabla} \times \boldsymbol{B} = \mu \left(\boldsymbol{J} + \epsilon \frac{\partial \boldsymbol{E}}{\partial t} \right) \tag{B.1a}$$

$$\boldsymbol{\nabla} \times \boldsymbol{E} = -\frac{\partial \boldsymbol{B}}{\partial t} \tag{B.1b}$$

$$\boldsymbol{\nabla} \cdot \boldsymbol{E} = \frac{\rho}{\epsilon} \tag{B.1c}$$

$$\boldsymbol{\nabla} \cdot \boldsymbol{B} = 0 \tag{B.1d}$$

We will now derive an equivalent set of differential equations. The maxwell equations are a set of four coupled first order differential equations and we will now write an equivalent system of two second order differential equations. We do this by defining two potentials: V (the scalar electric potential) and $\boldsymbol{A}$ (the magnet vector potential). We first define an expression for $\boldsymbol{B}$. Next, we use equation B.1b to find our potential. Define:

$$\boldsymbol{B} = \nabla \times \boldsymbol{A} \tag{B.2}$$

Equation B.1b yields:

$$\nabla \times \left(\boldsymbol{E} + \frac{\partial \boldsymbol{A}}{\partial t} \right) = 0 \tag{B.3}$$

This means that we can write:

$$\boldsymbol{E} + \frac{\partial \boldsymbol{A}}{\partial t} = -\nabla V \tag{B.4}$$

for a scalar potential V. We will now substitute equation B.4 into equation B.1c. This yields:

$$\nabla^2 V + \frac{\partial}{\partial t} \left(\nabla \cdot \boldsymbol{A} \right) = -\frac{\rho}{\epsilon} \tag{B.5}$$

We also substitute equation B.4 into equation B.1a. This yields:

$$\nabla^2 \boldsymbol{A} - \epsilon\mu \frac{\partial^2 \boldsymbol{A}}{\partial t^2} - \nabla \left(\nabla \cdot \boldsymbol{A} + \epsilon\mu \frac{\partial V}{\partial t} \right) = -\mu \boldsymbol{J} \tag{B.6}$$

We will now decouple the two equations above. From the definition of $\boldsymbol{B}$ it follows that $\boldsymbol{A}$ is arbitrary. This is shown in the following:

$$\nabla \times \boldsymbol{A} = \nabla \times (\boldsymbol{A} + \nabla\zeta) \tag{B.7}$$

This equation shows that the transformation from $\boldsymbol{A}$ to $\boldsymbol{A}+\nabla\xi$ does not change the induction vector $\boldsymbol{B}$. Now we have to choose a transformation for the electric potential V such that the electric field $\boldsymbol{E}$ does not change. We will use equation $B.4$ and substitute the transformation for $\boldsymbol{A}$:

$$\boldsymbol{E} = -\frac{\partial \boldsymbol{A}}{\partial t} - \nabla\left(\frac{\partial \xi}{\partial t} + V\right) \tag{B.8}$$

This means that we transform the scalar electric potential from V to $V - \frac{\partial \xi}{\partial t}$. We can now choose $\boldsymbol{A}$ and V such that:

$$\nabla \cdot \boldsymbol{A} + \epsilon\mu\frac{\partial V}{\partial t} = 0 \tag{B.9}$$

This yields:

$$\nabla \cdot \boldsymbol{A} = -\epsilon\mu\frac{\partial V}{\partial t} \tag{B.10}$$

By substituting this into equation $B.5$ and $B.6$, we get:

$$\nabla^2\boldsymbol{A} - \epsilon\mu\frac{\partial^2 \boldsymbol{A}}{\partial t^2} = -\mu\boldsymbol{J} \tag{B.11a}$$

$$\nabla^2 V - \epsilon\mu\frac{\partial^2 V}{\partial t^2} = -\frac{\rho}{\epsilon} \tag{B.11b}$$

These two equations and equation $B.9$ are equivalent to the set of Maxwell's equations stated in the first part of this paragraph. For our purposes the second-order time derivative can be neglected, because the time scale in which the device operates is much longer than the time it takes an electromagnetic wave to travel the length of the device. This yields poisson's equation for the scalar electric potential:

$$\nabla^2 V = -\frac{\rho}{\epsilon} \tag{B.12}$$

$$-\frac{1}{q}\nabla(\boldsymbol{J_p} - \boldsymbol{J}_n) = \frac{\partial}{\partial t}(p - n) \tag{B.13}$$

Appendix C

Experiments

At the department of Imaging Physics at the TU Delft, experiments are conducted to determine the secondary electron yield of certain materials. These measurements are done by Hong Chan Wah and for a detailed description of his experiments I refer to his "paper". With the results of his measurements the validity of the model described in chapter 2 can be determined. A short description of the experiments to determine the yield of a material is given in this chapter.

C.1 Experiment

Before the experiment can be properly described a few definitions have to be stated. The secondary electron yield is defined as follows:

$$\delta = \frac{N_s}{N_p} \tag{C.1}$$

Where N_p is the number of primary electrons (PE) and N_s the number of secondary electrons (SE). The source for our primary electrons is the electron canon in a scanning electron microscope (SEM). To measure the yield (δ) a device called the dual Faraday cup is used. In figure $C.1$ a schematic of the dual Faraday cup is shown. The setup as it is used now only makes use of the lower half of the dual Faraday cup. This is because the sample that is placed in electrode 3 cannot be imaged when the upper half is on top, this means that de electron beam cannot be focused. Furthermore is a small Faraday cup (SFC) placed in electrode 3. To each electrode a Keithley 2450 source-meter is connected. This allows the electrodes to be biased, while also making it possible to measure the current through the three electrodes. The yield can be determined by these currents as follows:

$$\delta = \frac{I_{SE}}{I_{PE}} \tag{C.2}$$

In this experiment we want to distinguish between reflected secondary electrons (RSE), transmitted secondary electrons (TSE) and forward/backward scattered electrons (FSE/BSE). Also the RSE and the BSE have to be distinguished.

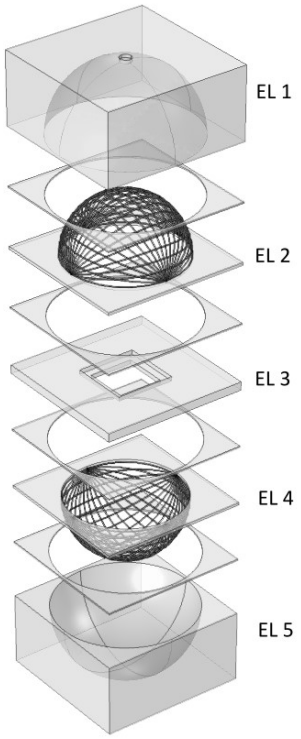

Figure C.1: Dual faraday cup. This image was taken from the report by Hong Wah

This also applies to TSE and FSE. Now we define a few yields. The reflected secondary electron yield is given by:

$$\delta_R = \frac{I_{RSE}}{I_{PE}} \tag{C.3}$$

The transmitted secondary electron yield by:

$$\delta_T = \frac{I_{TSE}}{I_{PE}} \tag{C.4}$$

Backscattered electron yield by;

$$\eta = \frac{I_{BSE}}{I_{PE}} \tag{C.5}$$

Forward scattered electron yield by:

$$\tau = \frac{I_{FSE}}{I_{PE}} \tag{C.6}$$

In every measurement $I_{PE} = I_{SFC}$, the current measured in de small faraday cup. Now two experiments have to be done to learn I_{TSE} and I_{FSE}. In the first experiment the sample will be negatively biased and in the second experiment the sample will be positively biased.

C.1.1 Negative bias

When the sample is negatively biased both the transmitted secondary electrons as the forward scattered electrons will be accelerated into the faraday cup and currents will be measured. The reflected secondary electrons and the backward scattered electrons will be accelerated into the SEM. This contribution will be called: I_{SEM}. We get:

$$I_{SFC} = I_{SEM} + I_3 + I_4 + I_5 \tag{C.7}$$

In this equation $I_{\#}$ is the current through electrode #. Because the TSE and the FSE are accelerated to the cup, the following is known:

$$I_4 + I_5 = [I_{TSE} + I_{FSE}] \tag{C.8}$$

The square brackets are used to show that I_{TSE} and I_{FSE} cannot be distinguished at this moment. The total yield of experiment 1 is given by:

$$\sigma_1 = [\delta_R + \eta] + [\delta_T + \tau] = \frac{I_{SEM}}{I_{SFC}} + \frac{I_4 + I_5}{I_{SFC}} \tag{C.9}$$

C.1.2 Positive bias

When the sample is positively biased all the low energetic electrons that are leaving the sample at the sample-vacuum interface get pulled back. This means that only the high energy backward/forward scattered electrons leave the sample. This means that:

$$I_{SEM} = I_{BSE} \tag{C.10}$$

and

$$I_4 + I_5 = I_{FSE} \tag{C.11}$$

The total yield is given by:

$$\sigma_2 = \eta + \tau = \frac{I_{BSE}}{I_{PE}} + \frac{I_{FSE}}{I_{PE}} = \frac{I_{SEM}}{I_{SFC}} + \frac{I_4 + I_5}{I_{SFC}} \tag{C.12}$$

The backscatter yield is given by:

$$\eta = \frac{I_{BSE}}{I_{PE}} = \frac{I_{SEM}}{I_{SFC}} = \frac{I_{SFC} - I_3 - I_4 - I_5}{I_{SFC}} \tag{C.13}$$

The forward scattered yield is given by:

$$\tau = \frac{I_{FSE}}{I_{PE}} = \frac{I_4 + I_5}{I_{SFC}} \tag{C.14}$$

By subtracting $sigma_2$ from $sigma_1$ we get:

$$\delta_R + \delta_T = \sigma_1 - \sigma_2 \tag{C.15}$$